Long-term measurements of ocean waves and sea ice draft in the central Beaufort Sea

Jim Thomson

Technical Memorandum

APL-UW TM 1-20
October 2020

ACKNOWLEDGMENTS

Funding for this work was provided by the Office of Naval Research (N00014-16-1-2349, N00014-13-1-0284, N00014-12-1-0113). Rick Krishfield and the mooring group at the Woods Hole Oceanographic Institution conducted all of the mooring work associated with these data, with help from the crew of the CCGC *Louis St. Laurent*. Sam Brenner, Lettie Roach, and Vince Cooper provided valuable feedback on the data products.

ABSTRACT

An ongoing program has measured ocean surface waves and sea ice draft at two sites in the Beaufort Sea (western Arctic Ocean) since 2012. This report presents the measurements and processed data products available from 2012 to 2018. Ocean surface waves are observed each summer and autumn when sea ice retreats; observed range of significant wave heights is 0.5–4 m. Sea ice is observed the rest of the year; observed range of average draft is 0.5–5 m.

Contents

1 INTRODUCTION

This report expands upon the work of *Thomson and Rogers* (2014), in which moored time series of ocean surface waves in the Beaufort Sea were used to show that the fetch distance from the mooring to the sea ice edge was the primary control on the wave height in the region. Subsequent studies have shown that wave heights in the Beaufort Sea are increasing as the seasonal sea ice retreat increases and expands the fetch distance (*Liu et al.*, 2016; *Thomson et al.*, 2016; *Wang et al.*, 2015). The data used in *Thomson and Rogers* (2014) were collected in 2012; the dataset has been continued and now extends to 2018. This report documents the extended dataset, which is publicly available at
`https://digital.lib.washington.edu/researchworks/handle/1773/15609`.

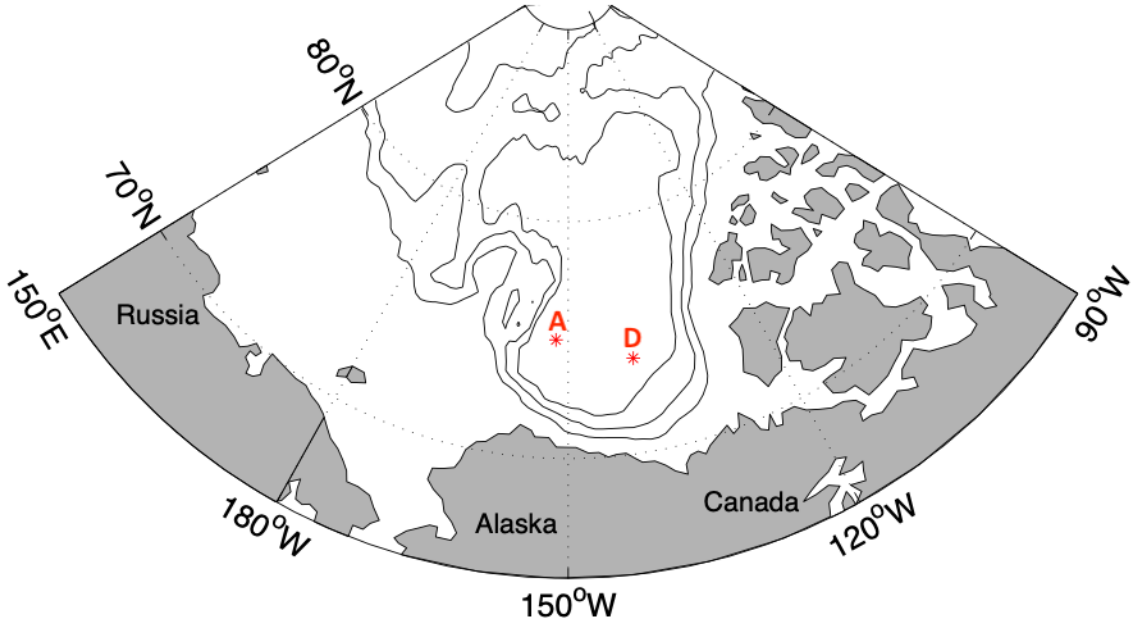

Figure 1: Location of moorings. Depth at each site is approximately 3000 m.

Figure 1 shows the locations of the data collection. The moorings are maintained by Rick Krishfield and colleagues at the Woods Hole Oceanographic Institution (WHOI) as part of the Beaufort Gyre Observing System (BGOS). BGOS is funded by the National Science Foundation as part of the Arctic Observing Network. The wave sensors are included as an informal collaboration using Office of Naval Research funding to APL-UW; they are not funded by NSF. The moorings were maintained annually until 2018, when the switch was made to biannual and then the COVID-19 pandemic prevented the scheduled recovery in 2020. More information on BGOS is available at `https://www.whoi.edu/beaufortgyre`.

Mooring	Location	2012–13	2013–14	2014–15	2015–16	2016–17	2017–18
BGOS-A	75°N, 150°W	y	y	n	y	y	y
BGOS-D	74°N, 140°W	n	y	y	n	y	y

Table 1: Mooring locations and data collections. Deployments generally start and end in September.

2 METHODS

Data were collected using Nortek Acoustic Wave And Current (AWAC, 600 kHz) instruments that were mounted upward looking on sub-surface moorings in the central Beaufort Sea (Figure 2). Once deployed, the instrument is approximately 30 m below the surface, though it can be as deep as 60 m when the mooring "blows down" during strong currents. The AWACs have four acoustic beams; the center beam functions as an altimeter to record sea surface elevations (i.e., waves) and ice draft.

Figure 2: Mooring during deployment. The AWAC is on the right-hand side (white and blue sonar head).

The AWACs sample sea surface elevations at 1 Hz for 1024 seconds at the beginning of each hour, then enter standby mode for the rest of the hour. After despiking, the raw wave data are processed following the methods of *Herbers et al.* (2012); *Kuik et al.* (1988); *Thomson et al.* (2018a). Scalar wave energy spectra are calculated from 256-second windows that are tapered and overlapped (50%) to form ensemble spectral energy densities $E(f)$. After merging every three neighboring frequency bands, the final spectra have 24 degrees of freedom and frequency resolution $df = 0.0117$ Hz.

The spectra are screened using a shape function, in which the frequencies $f > 0.3$ Hz are fit to a power law $E \sim f^q$ with the expectation that $q \leq -4$ for waves in open water or attenuated in ice (*Rogers et al.*, 2016). Any spectra with a fitted $q \geq -2$ indicate too much contamination by noise or ice in the raw data. Those values are assigned NaN in the dataset. Some of the remaining wave spectra do include times with ice cover, but only when the wave signal is clearly present. The wave spectra

are used to determine the significant wave heights for each hour as $H_s = 4\sqrt{\int E(f)df}$ and peak wave period T_p as the inverse of the frequency f_p at the maximum value of $E(f)$.

Figure 3 shows an example of raw data from the acoustic surface tracking (AST) and the pressure gage on the AWAC, as well as the spectra of these signals. The altimeter has two different algorithms (AST1 and AST2) to identify the surface; they are usually in agreement, with the exception of a few outliers in each. The outliers in the figure are single points that are not connected by lines in the time series; these are removed and assigned a running mean value before processing. The example spectra show excellent agreement, which is typical. The pressure measurements can also detect waves, but the signal is attenuated from the surface down to the $\sim$ 30 m depth of the instrument. A spectral function e^{-kz}, where k is the wavenumber from dispersion $(2\pi f)^2 = gk$, can be used to correct for this attenuation, after which the corrected pressure spectra are consistent with the AST spectra. However, the pressure spectra are often contaminated by noise at higher frequencies, and thus the AST spectra are used exclusively throughout this analysis.

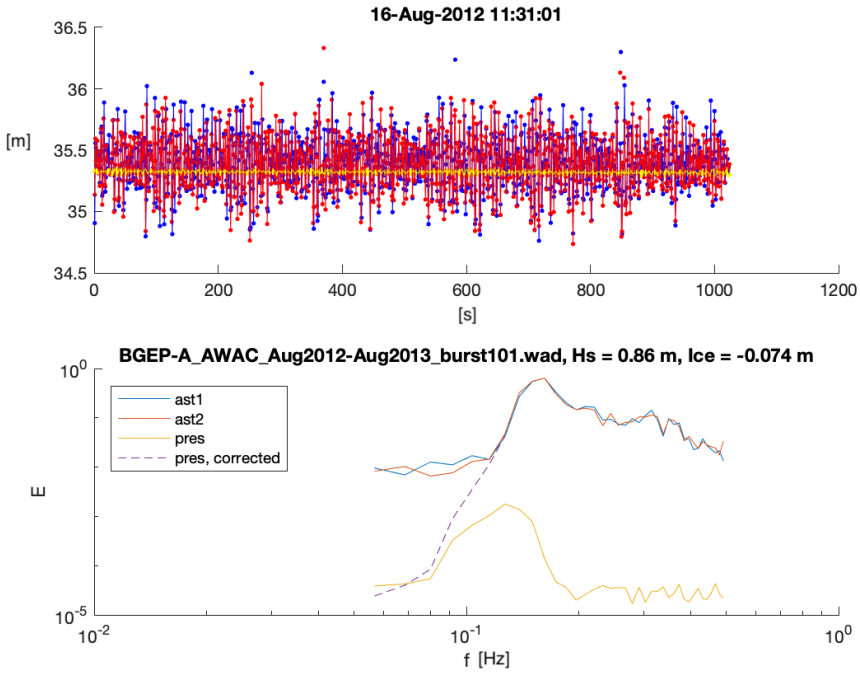

Figure 3: Example raw time series (1024 seconds) and computed frequency spectra from the AWAC measurements.

Previous work has validated AWAC measurements of waves relative to buoy mea-

surements in open water, including using the velocities from the three slanted beams to determine wave directions (*Pederson et al.*, 2007). This dataset is not suitable for estimating wave directional moments, because the horizontal magnetometer measurements of instrument heading at high latitudes are insufficient to transform the along-beam velocities into geographic components. Thus, the dataset only includes scalar wave estimates.

When sea ice is over the mooring, the ice drafts can be determined using the altimeter distance to the bottom of the ice relative to the instrument depth indicated by the pressure measurement (*Magnell et al.*, 2010). The dataset includes an ice draft value for each hourly burst, averaged over the burst length of 1024 seconds. Over this timescale, each burst can contain a mixture of level ice, leads, and ice keels, all of which will be retained in the average and likely skewing the average away from the value of the level ice draft. The dataset also includes histograms of ice draft from each set of 1024 measurements, with bin centers at $[0 : 0.5 : 10]$ m. Data are not used when the average depth exceeds 50 m during mooring blow-down or when the pitch and roll of the instrument exceed ± 5, because the acoustic altimeter cannot find the bottom of the ice reliably. Those values are assigned NaN in the dataset. Corrections for atmospheric pressure variations or instrument tilt (below ± 5) are not included (which together can give errors of approximately ± 0.2 m). The BGOS dataset at WHOI, which uses a different upward looking sonar (ULS) is the preferred source for ice draft data, following *Krishfield et al.* (2014). The AWAC dataset is secondary.

3 RESULTS

The full time series of wave heights and ice drafts is shown in Figure 4. As expected, waves are only present in the late summer and autumn (when there are significant regions of open water). Also as expected, the sea ice has a seasonal cycle in thickness, with an annual maxima in the later winter. It is important to consider the instrument operation and the ice results when interpreting the presence or absence of waves. In the summer of 2013, the AWAC on BGOS-A was operating, but it was covered by sea ice and no valid wave spectra were found. In the summer of 2014, the AWAC on BGOS-A was *not* operating (premature battery failure) and thus there are neither wave nor ice observations. From 2014 to 2015, the AWAC on BGOS-A was not deployed (because of the battery failure in the prior deployment). In the summer of 2014, the AWAC on BGOS-D was operating, but there is a gap in the observations between the end of one deployment and the beginning of the next. From 2015 to 2016, the AWAC on BGOS-D was not functioning (software error). These deployment anomalies are summarized in Table 1.

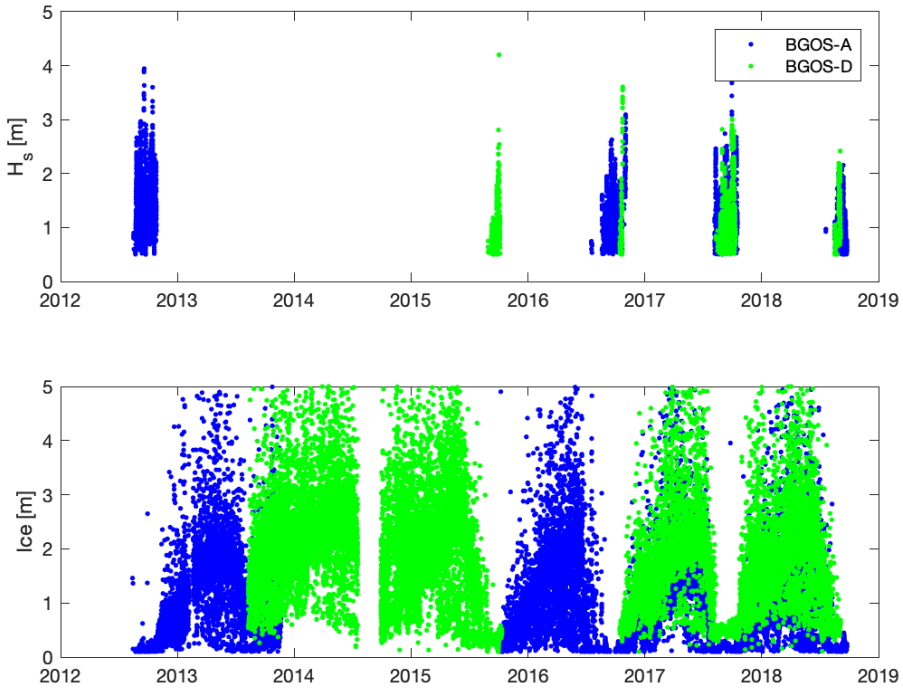

Figure 4: Full time series of wave heights and ice draft measurements.

Figure 5 shows merged histograms of wave heights and ice draft measurements from both moorings. Wave heights of 1 m are common; extremes are around 4 m. Ice drafts of 1–2 m are common, extremes are > 5 m. There are many more ice draft observations than wave height observations, because the open water season is relatively short.

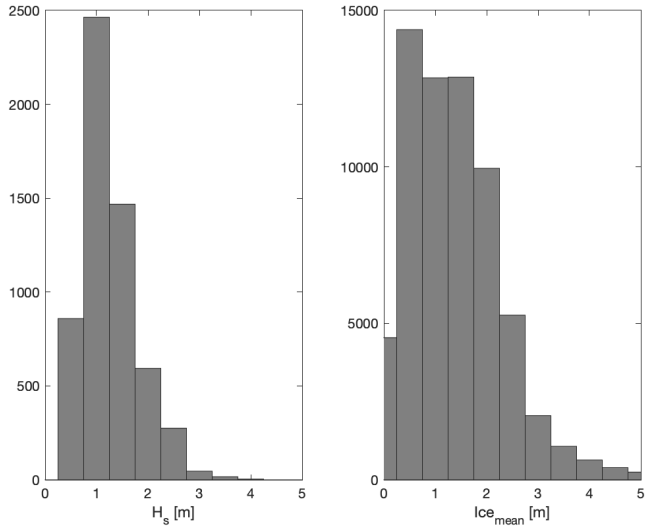

Figure 5: Merged histograms of wave heights and ice draft measurements from both moorings.

3.1 Wave Results by Year

For the years with valid wave observations, Figures 6–13 show detailed time series and wave spectra (as spectrograms). These reveal specific events, such as the storm in September 2012 reported by *Thomson and Rogers* (2014) or the storm in October 2015 included in analysis from the Arctic Sea State program (*Stopa et al.*, 2018; *Thomson et al.*, 2019, 2018b).

The time series of wave heights include a comparison to the ERA5 reanalysis model product. There is general agreement, though a rigorous statistical comparison is yet to be done.

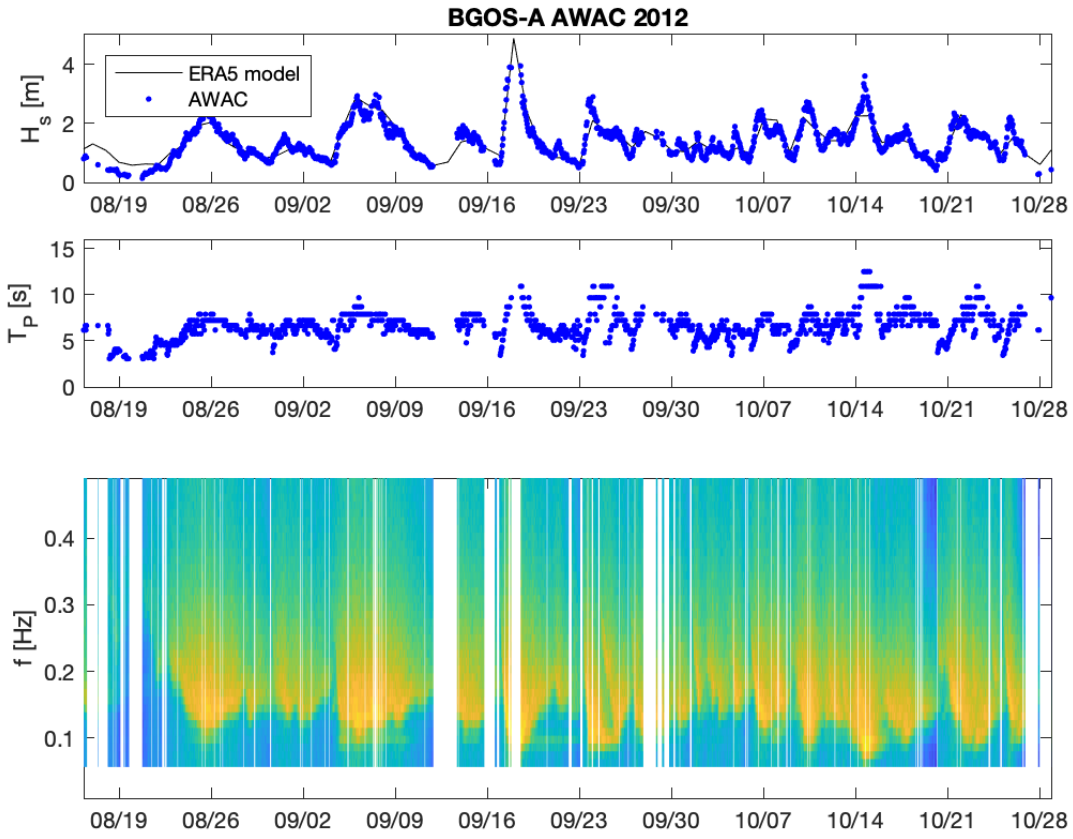

Figure 6: Significant wave heights, peak wave periods, and spectrograms (color is log_{10} of wave energy density) of waves from BGOS-A in 2012.

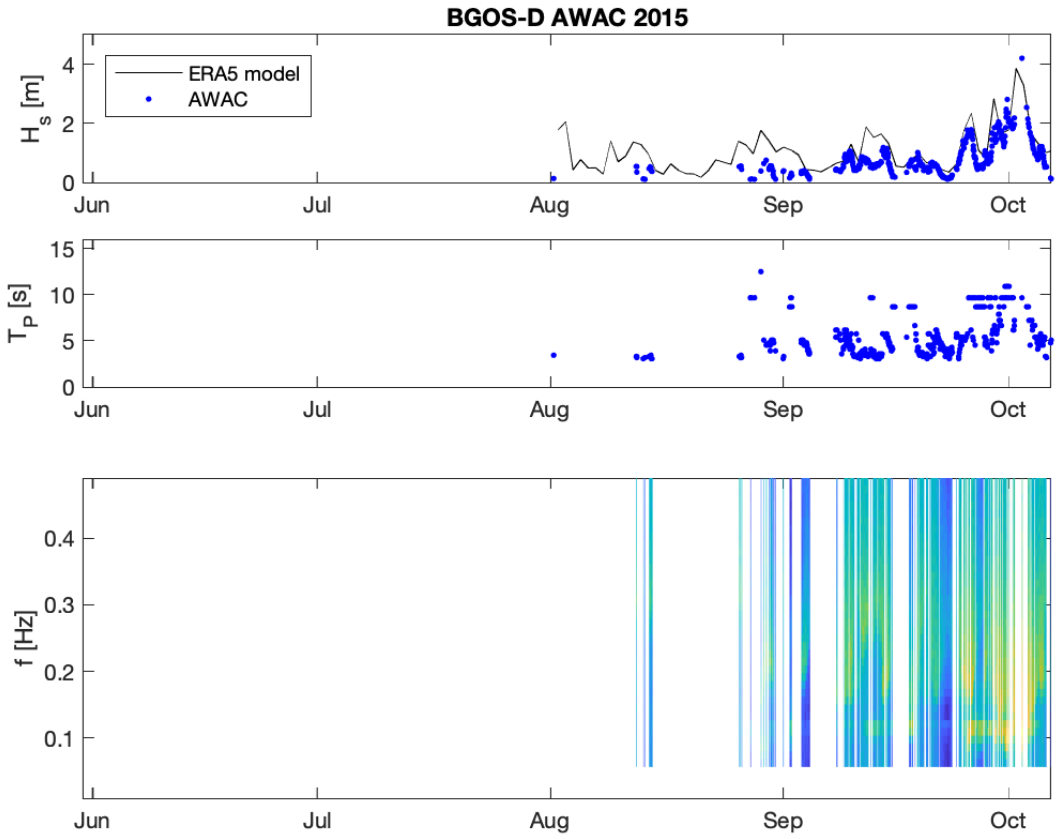

Figure 7: Significant wave heights, peak wave periods, and spectrograms (color is log_{10} of wave energy density) of waves from BGOS-D in 2015.

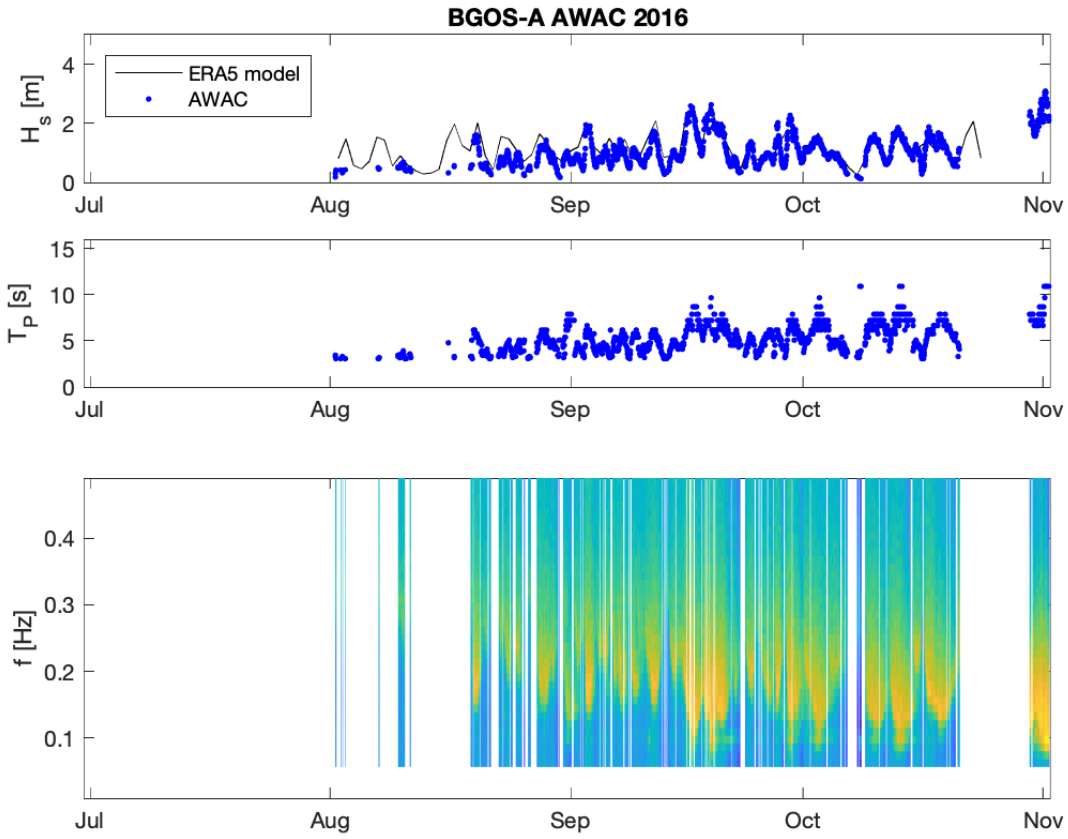

Figure 8: Significant wave heights, peak wave periods, and spectrograms (color is log_{10} of wave energy density) of waves from BGOS-A in 2016.

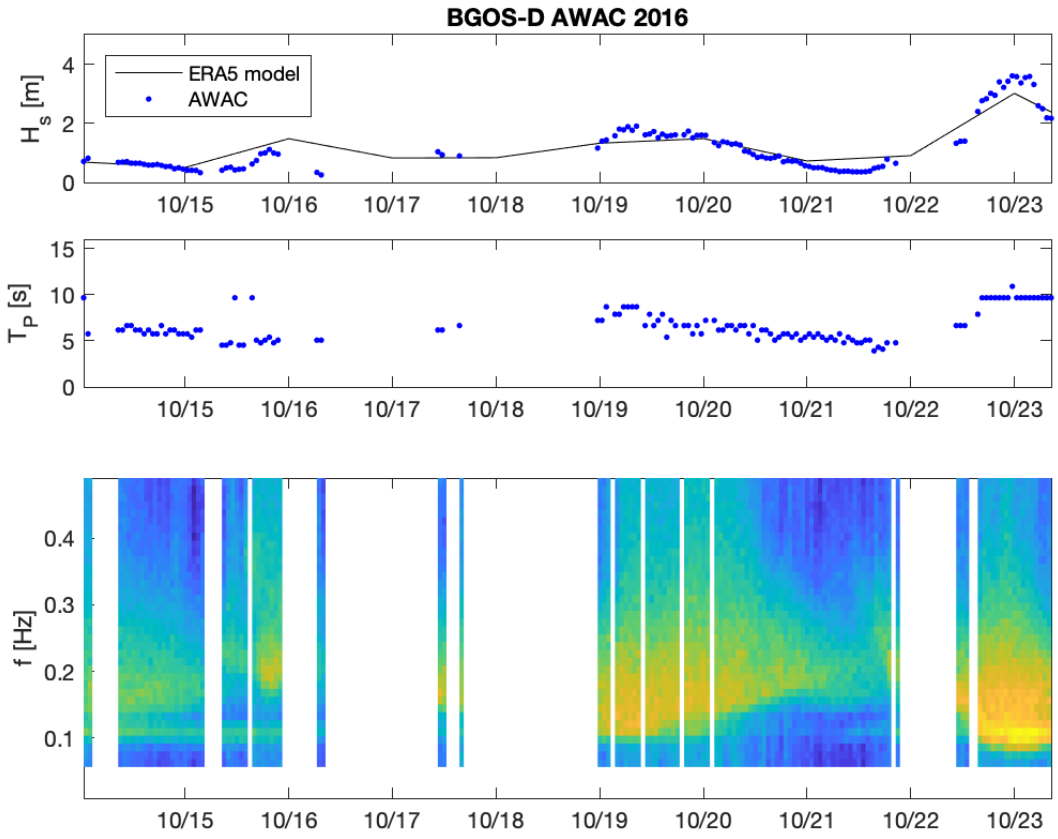

Figure 9: Significant wave heights, peak wave periods, and spectrograms (color is log_{10} of wave energy density) of waves from BGOS-D in 2016.

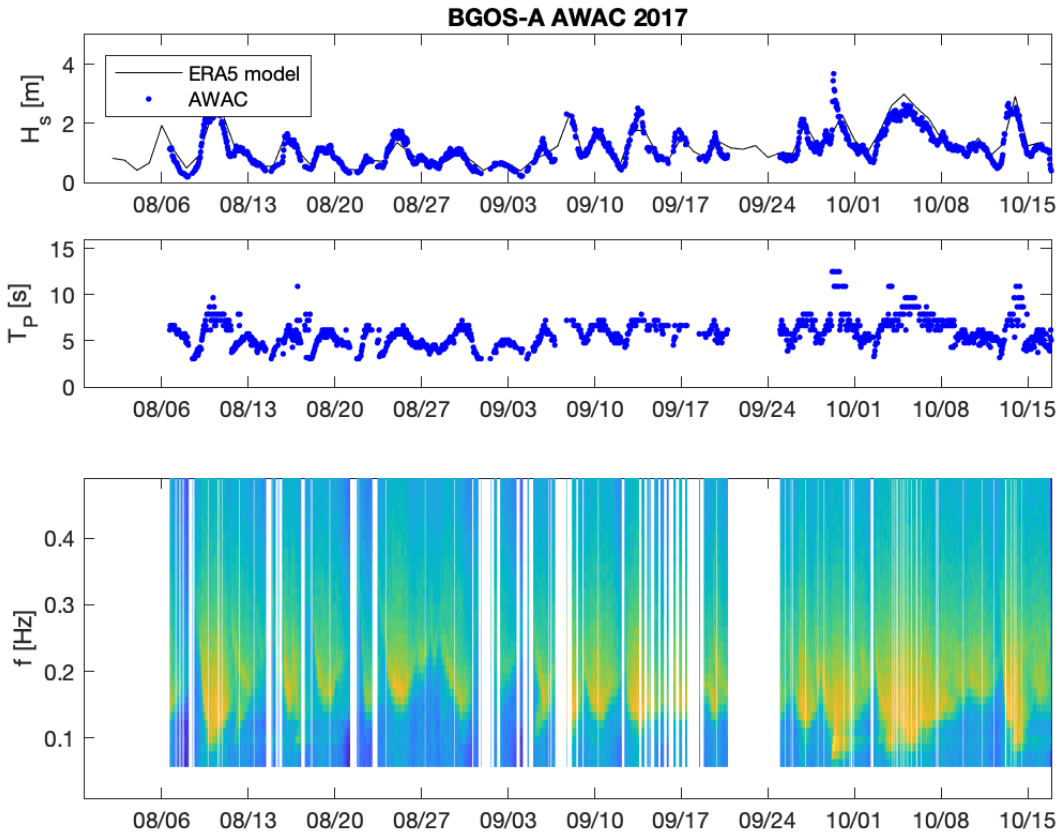

Figure 10: Significant wave heights, peak wave periods, and spectrograms (color is log_{10} of wave energy density) of waves from BGOS-A in 2017.

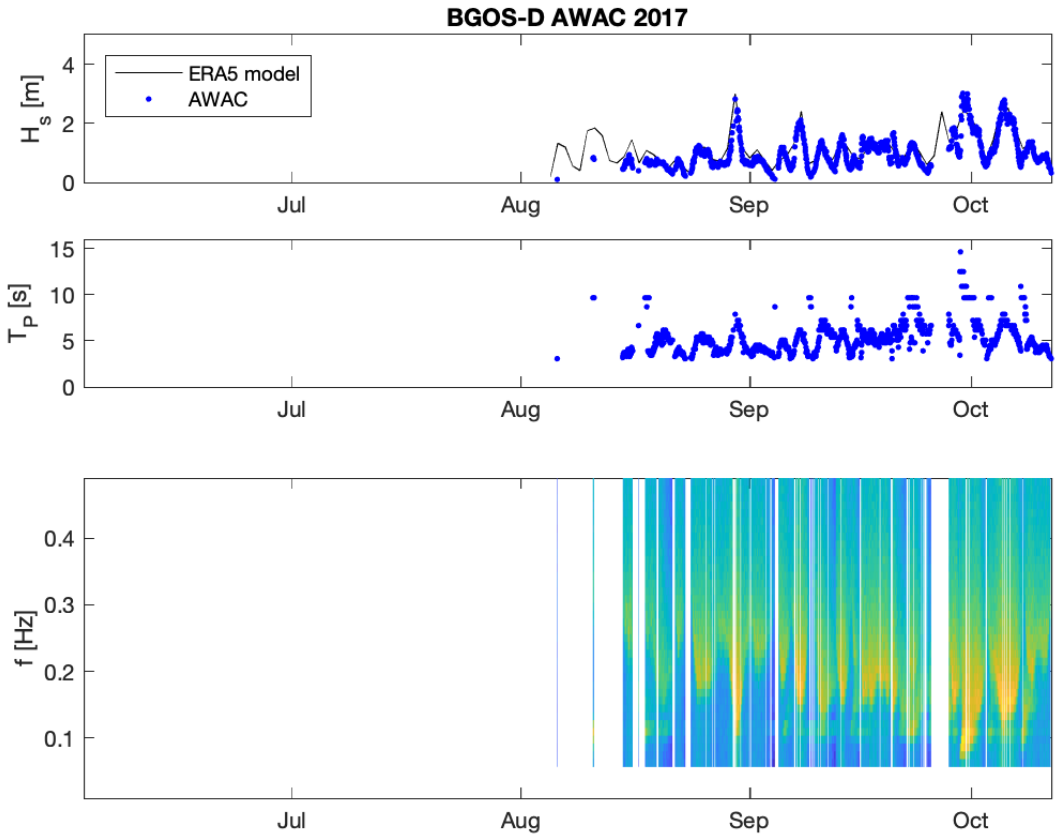

Figure 11: Significant wave heights, peak wave periods, and spectrograms (color is log_{10} of wave energy density) of waves from BGOS-D in 2017.

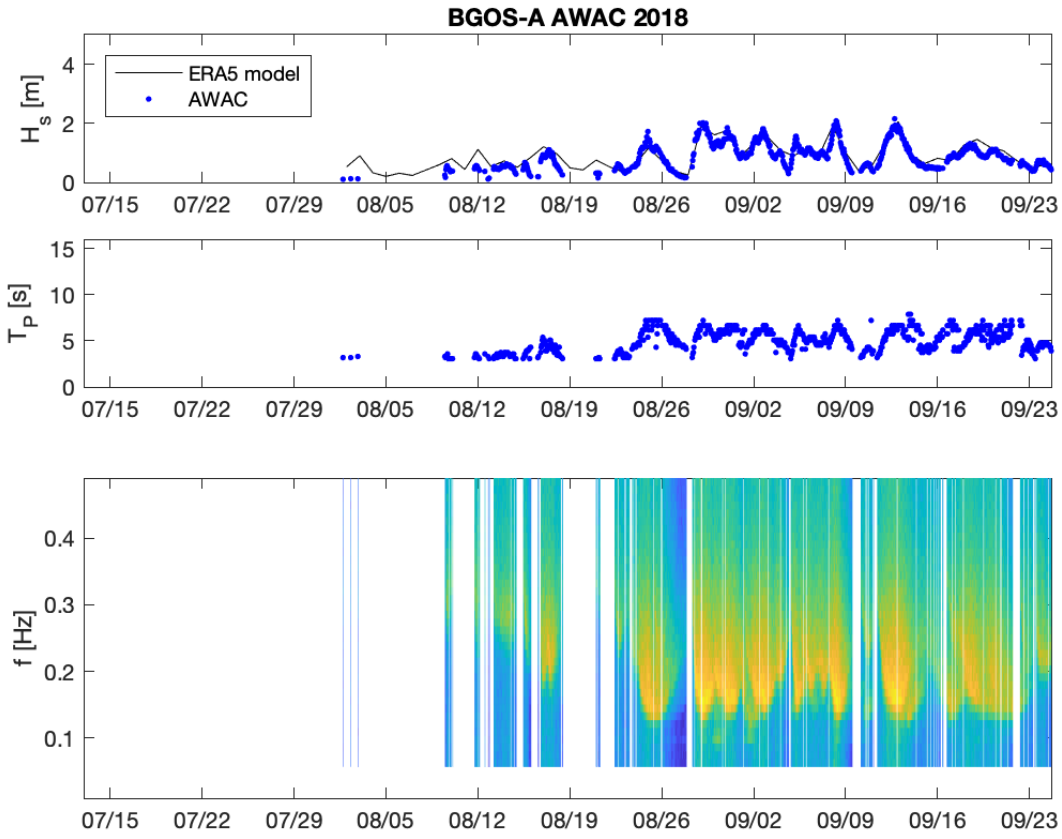

Figure 12: Significant wave heights, peak wave periods, and spectrograms (color is log_{10} of wave energy density) of waves from BGOS-A in 2018.

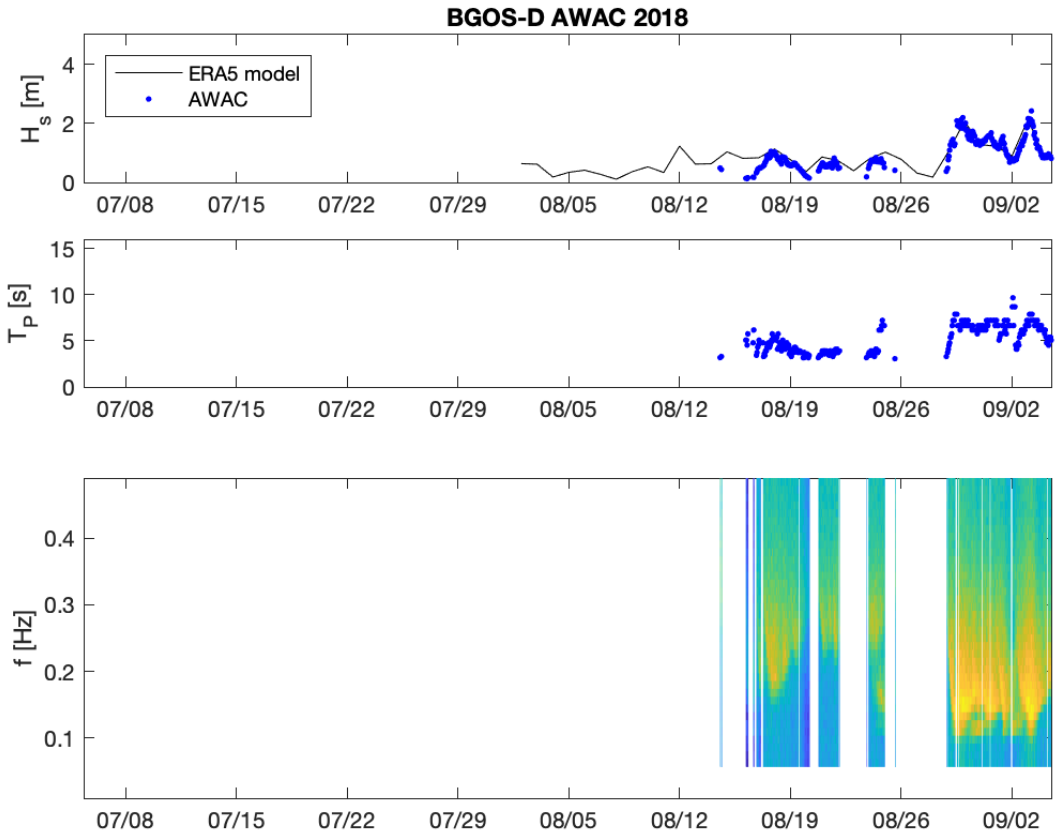

Figure 13: Significant wave heights, peak wave periods, and spectrograms (color is log_{10} of wave energy density) of waves from BGOS-D in 2018.

3.2 Ice Results by Year

Figures 14–15 show histograms derived from the hourly ice draft observations. The bins are centered every 0.5 m from 0 to 10 m and each contains $N = 1024$ total individual ice draft measurements as a burst of data each hour. The distributions generally are narrow with up to $N = 800$ measurements often in a single bin. The distributions are occasionally bimodal, especially in the spring and early summer, and this is consistent with seasonal leads opening in the sea ice.

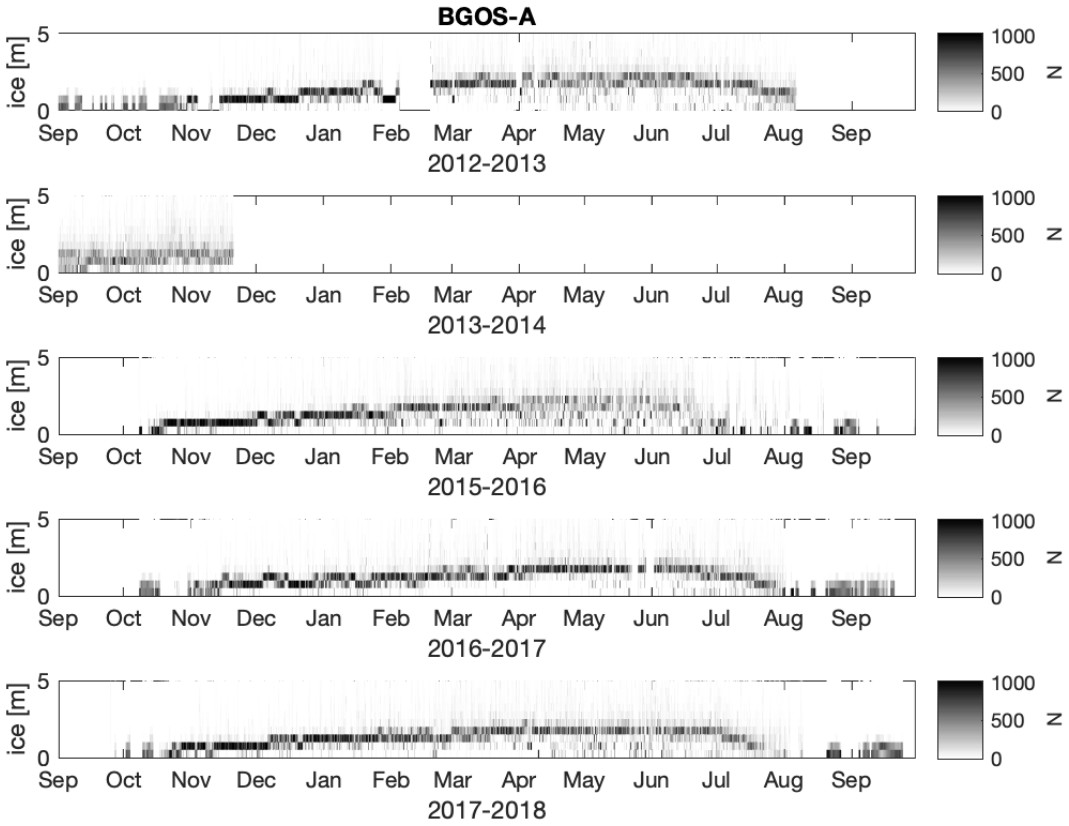

Figure 14: Time series histograms of ice drafts from BGOS-A. Each histogram consists of 1024 individual ice draft measurements.

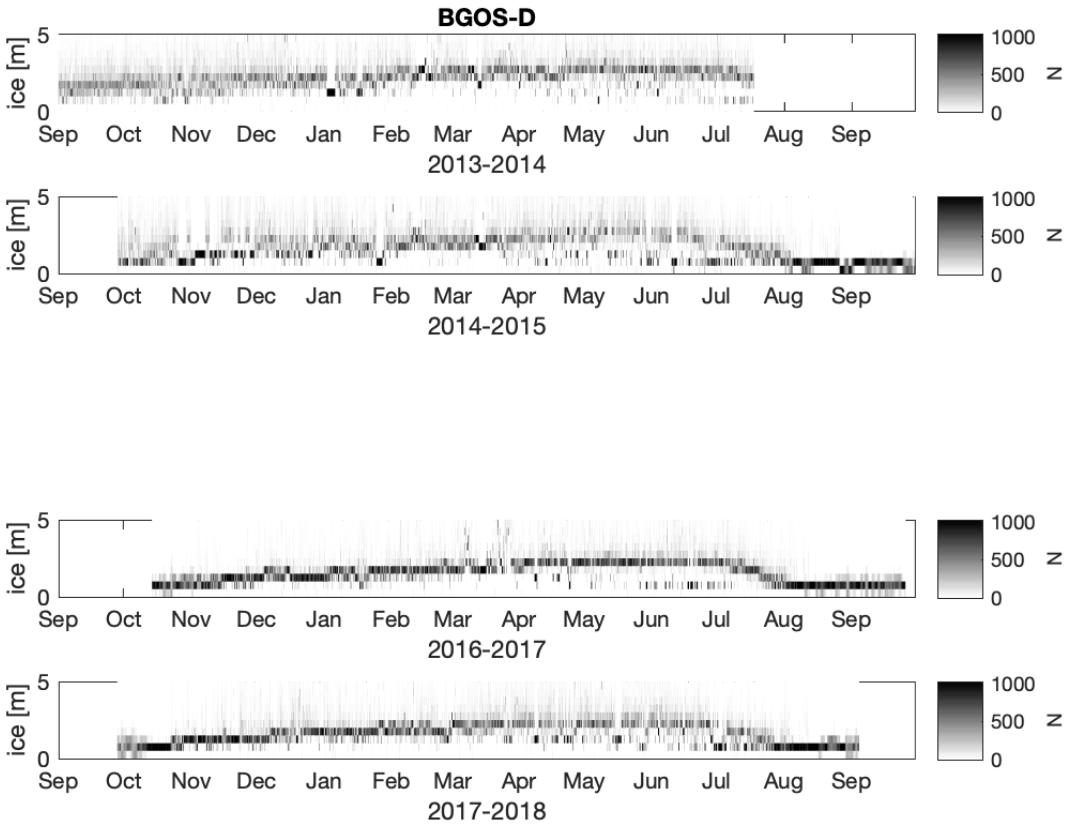

Figure 15: Time series histograms of ice drafts from BGOS-D. Each histogram consists of 1024 individual ice draft measurements.

4 CONCLUSION

A dataset of ocean waves initiated in 2012 and reported by *Thomson and Rogers* (2014) has been extend to 2018 and is available for public use. The dataset consists of seasonal ocean surface wave heights and spectra, along with sea ice draft from two locations in the central Beaufort Sea (western Arctic Ocean). A brief comparison with ERA5 model reanalysis shows that the model wave heights are consistent with the observations, including the emergence of large waves in the late autumn. The dataset is archived at
`https://digital.lib.washington.edu/researchworks/handle/1773/15609`.

REFERENCES

Herbers, T. H. C., P. F. Jessen, T. T. Janssen, D. B. Colbert, and J. H. MacMahan, Observing ocean surface waves with GPS tracked buoys, *J. Atmos. Ocean. Tech.*, *29*, doi:10.1175/JTECH-D-11-00128.1, 2012.

Krishfield, R. A., A. Proshutinsky, K. Tateyama, W. J. Williams, E. C. Carmack, F. A. McLaughlin, and M.-L. Timmermans, Deterioration of perennial sea ice in the Beaufort Gyre from 2003 to 2012 and its impact on the oceanic freshwater cycle, *J. Geophys. Res. Oceans*, *119*(2), 1271–1305, doi:10.1002/2013JC008999, 2014.

Kuik, A. J., G. P. V. Vledder, and L. H. Holthuijsen, A method for the routine analyis of pitch-and-roll buoy wave data, *J. Phys. Ocean.*, *18*, 1020–1035, 1988.

Liu, Q., A. V. Babanin, S. Zieger, I. R. Young, and C. Guan, Wind and wave climate in the arctic ocean as observed by altimeters, *Journal of Climate*, *29*(22), 7957–7975, doi:10.1175/JCLI-D-16-0219.1, 2016.

Magnell, B., L. Ivanov, and E. Siegel, Measurements of ice parameters in the Beaufort sea using the Nortek AWAC acoustic Doppler current profiler, in *Proceedings of the Oceans 2010 conference*, MTS/IEEE, Seattle, WA (USA), 2010.

Pederson, T., E. Siegel, and J. Wood, Directional wave measurements from a subsurface buoy with an acoustic wave and current profiler (awac), in *Proceedings Oceans 2007, Vancouver, Canada.*, 2007.

Rogers, W. E., J. Thomson, H. H. Shen, M. J. Doble, P. Wadhams, and S. Cheng, Dissipation of wind waves by pancake and frazil ice in the autumn beaufort sea, *Journal of Geophysical Research: Oceans*, *121*(11), 7991–8007, doi:10.1002/2016JC012251, 2016.

Stopa, J. E., F. Ardhuin, J. Thomson, M. M. Smith, A. Kohout, M. Doble, and P. Wadhams, Wave attenuation through an arctic marginal ice zone on 12 october 2015: 1. measurement of wave spectra and ice features from sentinel 1a, *Journal of Geophysical Research: Oceans*, *123*(5), 3619–3634, doi:10.1029/2018JC013791, 2018.

Thomson, J., and W. E. Rogers, Swell and sea in the emerging Arctic Ocean, *Geophysical Research Letters*, pp. n/a–n/a, doi:10.1002/2014GL059983, 2014.

Thomson, J., M. S. Schwendeman, S. F. Zippel, S. Moghimi, J. Gemmrich, and W. E. Rogers, Wave-breaking turbulence in the ocean surface layer, *Journal of Physical Oceanography*, *46*(6), 1857–1870, doi:10.1175/JPO-D-15-0130.1, 2016.

Thomson, J., J. B. Girton, R. Jha, and A. Trapani, Measurements of directional wave spectra and wind stress from a wave glider autonomous surface vehicle, *Journal of Atmospheric and Oceanic Technology*, *35*(2), 347–363, doi: 10.1175/JTECH-D-17-0091.1, 2018a.

Thomson, J., J. Gemmrich, W. E. Rogers, C. O. Collins, and F. Ardhuin, Wave groups observed in pancake sea ice, *Journal of Geophysical Research: Oceans*, *124*(11), 7400–7411, doi:10.1029/2019JC015354, 2019.

Thomson, J., et al., Overview of the arctic sea state and boundary layer physics program, *Journal of Geophysical Research: Oceans*, *123*(12), 8674–8687, doi:10.1002/2018JC013766, 2018b.

Wang, X. L., Y. Feng, V. R. Swail, and A. Cox, Historical changes in the Beaufort-Chukchi-Bering seas surface winds and waves, 1971-2013, *Journal of Climate*, doi: 10.1175/JCLI-D-15-0190.1, 2015.